Parallaxes of five L Dwarfs with a Robotic Telescope

Y. Wang[1,2,3],

youfenwang@shao.ac.cn

H.R.A. Jones[3],

h.r.a.jones@herts.ac.uk

R.L. Smart[4],

smart@oato.inaf.it

F. Marocco[3],

federico.marocco@gmail.com

D.J. Pinfield[3],

d.j.pinfield@herts.ac.uk

Z. Shao[1,10],

zyshao@shao.ac.cn

I.A. Steele[5],

ias@astro.livjm.ac.uk

Z. Zhang[3],

z.zhang7@herts.ac.uk

A.H. Andrei[4,6],

oat1@on.br

A.J. Burgasser[9],

ajb@mit.edu

K.L. Cruz[7,8],

kelle.cruz@hunter.cuny.edu

J. Yu[1,2],

yujc@shao.ac.cn

J.R.A. Clarke[11],

jraclarke@hotmail.com

C.J. Leigh[5],

cjl@astro.livjm.ac.uk

A. Sozzetti[4],

sozzetti@oato.inaf.it

D.N. Murray[3],

D.Murray@herts.ac.uk

& B. Burningham[3],

b.burningham@herts.ac.uk

[1]Shanghai Astronomical Observatory, Chinese Academy of Sciences, 80 Nandan Road, Shanghai, 200030, China.

[2]University of Chinese Academy of Science, 19 Yuquan Road, Shijingshan District, Beijing, 100049, China

[3]Center for Astrophysics Research, University of Hertfordshire, Hatfield AL10 9AB,UK

[4]INAF/Osservatorio Astrofisico di Torino, Strada Osservatorio 20, 10025 Pino Torinese, Italy

[5]Astrophysics Research Institute, Liverpool John Moores University, Liverpool, CH41 1LD, UK

[6]Observatório Nacional/MCT,R, Gal. José Cristino 77,CEP20921-400,RJ, Brazil

[7]Dept. of Astrophysics, American Museum of Natural History, 79th St at Central Park West, New York, NY 10024

[8]Dept. of Physics and Astronomy, Hunter College, City University of New York, 695 Park Avenue, New York, NY 10065

[9]Center for Astrophysics and Space Science, University of California San Diego, La Jolla, CA 92093

[10]Key Laboratory for Astrophysics, Shanghai 200234, China

[11]Departamento de Físicay Astronomía, Facultad de Ciencias, Universidad de Valparaíso, Av. Gran Bretaña 1111, Playa Ancha, Casilla 5030, Valparaíso, Chile

ABSTRACT

We report the parallax and proper motion of five L dwarfs obtained with observations from the robotic Liverpool Telescope. Our derived proper motions are consistent with published values and have considerably smaller errors. Based on our spectral type versus absolute magnitude diagram, we do not find any evidence for binaries among our sample, or, at least no comparable mass binaries. Their space velocities locate them within the thin disk and based on the model comparisons they have solar-like abundances. For all five objects, we derived effective temperature, luminosity, radius, gravity and mass from a evolutionary model(CBA00) and our measured parallax; for three of the objects, we derived their effective temperature by integrating observed optical and near-infrared spectra and model spectra(BSH06 or BT-Dusty respectively) at longer wavelengths to obtain bolometric flux and then using the classical Stefan-Boltzmann law: generally the three temperatures for one object derived using two different methods with three models are consistent, while at lower temperature(e.g. for L3) the differences among the three temperatures are slightly larger than that at higher temperature(e.g. for L1).

Subject headings: stars: brown dwarfs, parallax, proper motion — Data Analysis and Techniques

1. Introduction

L-type dwarfs are ultracool objects cooler than M dwarfs. Most L dwarfs are expected to be brown dwarfs, i.e., have insufficient mass to achieve the central temperatures and pressures necessary for sustained hydrogen burning. Brown dwarfs have physical properties intermediate between the least massive stars and the most massive planets and are thus a useful bridge between studies of stars and planets (Burgasser 2011). However, the lack of a unique age - mass - spectral type relationship leads to distance being a critical parameter to understand brown dwarfs. A distance is required to derive an absolute magnitude and hence energy output. Parallaxes are a model independent parameter that can be used to constrain radius or temperature thus allowing modeling to explore relations between other parameters, mass - surface gravity- age - metallicity, more freely. Considering that distances are so valuable, it is a sign of the difficulty in obtaining them that out of more than 900 known L dwarfs (www.dwarfarchives.org hereafter DwarfArchive) less than 90 have measured parallaxes and, when this programme started, there were less than 20.

Here we discuss the determination of parallax and proper motion for five L dwarfs using the robotic Liverpool Telescope[1] (hereafter LT, Steele et al. 2004). In general, the observations required for parallax determinations are quite simple and routine. The important characteristics for observations in a parallax program are stability in the instrumental setup and repeatability in the observational procedure. The rigorous scheduling criteria, efficient use of time, flexibility in scheduling, and, observational consistency in robotic observations make it a very attractive possibility for parallax programs. This program was envisioned to see if the LT could become an exemplar parallax machine for future parallaxes of bright brown dwarfs and nearby red dwarfs. The number of brown dwarfs is increasing rapidly with continued discoveries from wide-field sky survey

---

[1]telescope.livjm.ac.uk

program, e.g., SDSS (York et al. 2000), VISTA (Emerson 2001), CFHT (Monin et al. 2007), UKIRT (Lawrence et al. 2007), and WISE (Wright et al. 2010) surveys. Many of these are observable with the LT.

This paper is divided into seven sections. In Section 2 we describe the observations and data reduction procedures. In Section 3 we report the main astrometric results. In Section 4 we study the binarity, Galactic membership, metallicity and gravity properties using spectral type - absolute magnitude, U-V velocity and color- absolute magnitude with model tracks diagrams. In Section 5 we present the bolometric flux, luminosity and effective temperature of our targets obtained combining our measured parallaxes with the optical/infrared spectra and evolutionary/atmospheric models. In Section 6 we comment on individual objects and in Section 7 we summarize our findings and briefly describe our future work plan.

2. Observations and reduction procedures

The LT is a totally robotic telescope located at the Observatorio del Roque de Los Muchachos on the Canary island of La Palma in Spain and operated by the Liverpool John Moores University in the United Kingdom. It is an Alt-Az telescope with Ritchey-Chretien Cassegrain optics with a primary mirror of 2.0 m. In 2004, when this parallax program started, there were two instruments that were suitable for a brown dwarf parallax program: SupIRCam and RATCam. SupIRCam is an infrared sensitive 256x256 pixel HgCdTe array with a pixel scale of 0.413 arcsecond/pixel and a field of view of 1.7 arcmin. RATCam is an optically sensitive 2048x2048 pixel CCD camera with a pixel scale of 0.1395 arcsecond/pixel and a field of view of 4.6 arcmin. The SDSS-z filter (hereafter simply z) corresponds to the brightest optical magnitude for L dwarfs. The larger field, smaller pixel scale and similar required exposure times for typical L dwarfs of the RATCam instrument in the z band filter

compared to the SupIRCam in the J filter led to RATCam being the preferred choice for our program.

2.1. Targets

The target list was selected from the literature with the following criteria: visible to the LT, a z band magnitude brighter than 18, no published trigonometric parallax in 2004 and those objects with the smallest photometric distance were preferred. Here we report on the five that have enough observations spread over 2004/2005, 2008/2009 and 2011/2012 to provide reliable parallaxes. In Table 1 we list the five objects with their z, and estimated z, 2MASS JHK (Skrutskie et al. 2006) and WISE $W1$ (Wright et al. 2010) band magnitudes, optical and near-infrared spectral types.

2.2. Observational procedure

The five targets were observed between August 2004 and July 2012 using RATCam with the z band filter. In order to minimize the effect of differential color refraction, we observe when the targets are within 30 minutes of the meridian. The observations were primarily made during twilight hours, since this is when the objects have maximum parallax factors in right ascension. Observed this way, the data are primarily located on the ends of the major semi-axis of their parallax ellipse. During each observation we take three exposures of 160s to allow for robust removal of cosmic rays and to diminish the random errors. One exposure of this length nominally provides a signal-to-noise of more than 50 on these targets.

Differential color refraction (DCR, Monet et al. 1992; Stone 2002) is the small varying displacement of objects with different colors in a field that results from the variation of

the atmosphere refractive index with wavelength. It is strongest in the blue bands and gradually gets very small in the infrared. The targets in this parallax program are redder than the anonymous reference objects so this displacement is systematically different from the average of those reference objects. We request that all our observations are made within 30 minutes of the meridian so the variation in airmass, and hence differential movement, is minimized. In the Torino Observatory Parallax Program (hereafter TOPP, Smart et al. 1999) we found the effect was very small in the I band and it will be smaller for the z band, though L dwarfs are redder than the TOPP targets. In the work by Dahn et al. (2002) they do not include DCR terms as they found they changed the z band parallax of L and T objects by only 0.3 mas. In Albert et al. (2011) they also found the DCR in the z band on relative astrometry of brown dwarfs was small enough to neglect. Following these results, and in light of our observational criteria, we have not included DCR terms in this analysis. For future work we will carry out a number of experiments to measure the DCR in the LT z band system and review this decision.

2.3. Reduction Procedures

The bias subtraction, trimming of the overscan regions, dark subtraction and flat fielding are carried out via the standard LT pipeline (Steele et al. 2004). However, images in the z band display prominent fringes caused by thin-film interference (see Appendix A in Berta et al. 2008). Fringes have a small effect on the photometry and astrometry for bright objects, but can have a significance impact for faint objects when their fluxes are comparable with the intensity of the fringes. Since our targets are relatively faint, we must investigate the impact of fringes.

To examine the intensity and evolution of the fringes we divide the images into three sub-samples: (1) 2004/2005, (2) 2008/2009 and (3) 2011/2012 images. Each sub-sample

contains several hundreds of frames. For each frame in each sub-sample we pick out an empty area (of 100×100 pixels) which is seriously fringed but without any or with very few objects. We calculate the RMS of the counts and average the values within each sub-sample. We find the count variations before and after defringing are 11.2 and 9.5, 8.1 and 6.8, 8.6 and 7.5 respectively for the three subsets, a difference that we consider significant.

The standard LT pipeline constructed biannual fringe maps and our first attempt was to use the most appropriate for each night. However, fringes are dependent on the sky conditions at the time of observation and vary during the course of a night. The ideal case would be to make a fringe map for each image, but this is not feasible. In addition we usually only have a few images in any given night so even a per night fringe map is not possible. Our second attempt was to construct fringe maps following the recipe in Andrei et al. (2011) for subsets of 20-30 frames while attempting to keep nights and periods covered intact. Using the fringe maps constructed by ourselves usually gave similar parallax results to those using the LT fringe map except in the case of the fainter targets. This is probably due to the fact that sometimes to have sufficient frames to construct a fringe map we had to include a relatively long time-span but with few frames compared to the LT fringe maps. The results presented here used the LT fringe maps which also produced more robust parallax solutions.

2.4.   Centroid Precision

Since our targets are faint and our data impacted by fringes which we can not remove completely, it is critical to have appropriate centroiding software in order to determine their position which is the fundamental data for a parallax determination. We tried several different methods: (1) two-dimensional Gaussian fit to the point spread function as used in the TOPP, (2) the widely used Sextractor routine which is

designed for large scale galaxy surveys and also works well on moderately crowded star fields (http://www.astromatic.net/software/sextractor) and (3) the maximum likelihood barycenter as implemented in the imcore software of the Cambridge Astronomy Survey Unit (CASU, http://casu.ast.cam.ac.uk/surveys-projects/software-release).

We tested all the centroiding procedures by comparing object positions from 57 frames of the 2M1807+5015 field. The centroiding was also tested with different defringing procedures. We found that for brighter objects we get similar results but CASU imcore centroids work significantly better for the fainter ones giving smaller errors. If we do not defringe, the median σ_x ,σ_y for the x,y coordinates are 25,28 mas for all objects, and 13,14 mas for objects brighter than magnitude z=17. Applying the fringe map provided by LT pipeline we find that the precision improves to 21,21 mas and 11,11 mas respectively. In Fig. 1 we present the standard deviations of the object coordinates in the 2M1807+5015 sequence defringed with the LT biannual fringe maps and centroided with the CASU routines.

Based on our experience in other parallax programs we expected to achieve a lower floor than 11,11 mas for the centroiding precision. We note that the RATCam CCD has electronic gates aligned with x axis and physical gates aligned with y axis. The precision from electronic gates is better than the physical gates. The source of this higher noise is probably because that nominally x is orientated in the direction of RA and y in Dec, but due to flexibility problems with the RATCam coolant pipes it was not possible to always keep the same alignment. A procedure of "cardinal pointing" is adopted that aligns the rotator to one of the four cardinal positions: 0, 90, 180 and 270. A third of our observations have the rotator aligned to 0, that is with North at top, East at left. The other images are evenly distributed between the other cardinal points, except during the first year of observation when there are also non-standard positions with a number of different angles.

Since the astrometric distortion is partially a function of the focal plane variations, this physical rotation of the focal plane impacts negatively on the expected precision. The new Infrared-Optical camera on the LT does not have this constraint.

Another possible source for this high floor is that our observations for 2M1807+5015 covered several years and there will be a small contribution from random proper and parallactic motion of the reference stars. Since we expose three times for each target in each night the precision using these three frames excludes this random motion contribution. There are 3 observations on 19 nights so we have 19 sub-groups with 3 frames in each. For each sub-group we calculated their median σ_x, σ_y for all objects and for objects brighter than z=17. In Fig 2 we plot the sigma versus epoch, the median precision for the objects brighter than z=17 improved to 3.8,3.7 mas. As each sample comprises of only three images we expect this to be an underestimate of the true sigma but it supports our hypothesis of the contribution from random motions. Since our parallax solutions come from the combined data-sets we must include the instrumental and reference system variations, so considering consistency of the final and per-epoch errors we assume an observational precision of 11,11 mas.

3. Parallaxes and Proper Motions

Using the x,y coordinates determined from the CASU imcore software we derived the parallaxes and proper motions using the methods adopted in the TOPP (Smart et al. 2003, 2007). The software selects the frames and reference stars automatically, for example frames with less than four reference stars in common, or, stars with large errors or high proper motions, are dropped. A base frame is selected in the middle of the sequence with a high number of stars. This base frame is transferred to a standard coordinate system using objects in common with 2MASS. The other frames are then transferred to this system using

all common stars with a linear transformation. Then by fitting the combined observations of the target in the standard coordinate system we find its relative parallax and proper motion. The correction from relative to absolute parallax is calculated using the galaxy model of Mendez & van Altena (1996) as described in Smart et al. (2003). We estimate the error on this correction to be around 30% or 0.4-0.6 mas for these fields (Smart et al. 2007), which is negligible compared to the formal error of the parallaxes.

In Table 2 we list our results and in Fig. 3 we plot the solutions for the targets 2M1807+5015 and SD1717+6526 which have respectively the lowest and highest parallax errors. As shown in Fig. 1 the centroiding deteriorates significantly as the object gets fainter. This is reflected in the correlation of derived parallax precision with apparent magnitude in Tables 1 and 2 and explains the noisier observations of SD1717+6526.

4. Analysis of properties

In this section we examine the physical characteristics of our objects using our parallax and proper motion results and taking advantage of two different brown dwarf models.

4.1. Absolute magnitude and spectral type interpretation

In Fig. 4 we plot the optical spectral type versus absolute magnitude diagram in J, H and K bands including our objects and published objects with measured parallaxes from Dupuy & Liu (2012). The solid red lines are the polynomial fit from M8 to T0 including our five L dwarfs and the published objects but excluding known and possible binaries. The magnitudes are 2MASS values and the spectral types are from optical spectra. We also include the Dupuy & Liu (2012) spectral type versus absolute magnitude relation and note that our targets and fit (solid red lines) are slightly below their relation (dashed

lines). In Table 3 we compare the Dupuy & Liu (2012) spectrophotometric distances with our trigonometric ones, and the two distances for the five L dwarfs are generally consistent within one sigma. Our trigonometric distance are generally slightly smaller, however, with such a small sample it is not possible to draw any conclusions.

In Table 5 we list the coefficients and errors of the fit to the polynomial:

$$M_X = \sum_{i=0}^{6} a_i x(SpT)^i \tag{1}$$

where SpT indicates the spectral type, following the convention M0 = 0, ...L0 = 10, ... T0 = 20, and M_X is the absolute magnitude in the X band where X=2MASS J, H or K. The fit is valid only in the SpT range from M8 to T0.

If any of our targets are unresolved binaries they will be brighter than a single object in Fig. 4. This brightening reaches a maximum for equal-mass binaries with an expected difference of 0.75 mag. Since this is not the case, we conclude none of the five targets consist of comparable mass binaries.

4.2. Kinematic analysis

The velocities of nearby objects are dominated by their rotation around the Galactic center. But they also have peculiar motions of several tens of km/s. In the Galactic coordinate system, this spatial motion can be described using U, V and W velocities, with the U axis oriented towards the Galactic anti-center. Different stellar populations such as disk objects or halo objects have particular distributions in U, V and W velocity space. So, if we can obtain the U, V and W of an object, we can kinematically determine which Galactic component it belongs to.

We convert proper motion, parallax and radial velocity into U, V and W velocities listed in Table 6. All velocities are corrected to the LSR adopting the solar motion $U_\odot$,

$V_{\odot}$, $W_{\odot}$ = 11.10, 12.24, 7.25 (Schonrich, Binney & Dehnen 2010). Only two objects, 2M0141+1804 and 2M1807+5015, have published radial velocity data (24.7 and -0.4 km/s), obtained from high resolution spectroscopy (Blake, Charbonneau & White 2010). For the other objects we assume their radial velocity distribution is similar to M dwarfs and we can then estimate their membership statistically as described below.

We select 18563 nearby M dwarfs within 500 pc from the West et al. (2011) spectroscopic catalog of $\sim$ 70000 M dwarfs from the SDSS DR7 which have measured radial velocity and spectrophotometric distances for each star. The radial velocity distribution of this sub-sample follows a Gaussian profile with the mean velocity $\sim$ 0 km/s and $\sigma \sim$ 30 km/s.

We use a check from Oppenheimer et al. (2001) to identify their membership in the different Galactic components. Objects that satisfy $[U^2 + (V + 35)^2]^{1/2} > 94$ km/s are considered halo objects at the 2σ level. In the U-V diagram Fig.5, we find 2M0141+1804 and 2M1807+5015 both locate within the 2σ circle. Which means the two targets are probably disk objects. We assume that the other three L dwarfs without measured radial velocity have velocities which follow the Gaussian distribution of the SDSS M dwarfs' as described above and then plot their U and V projection along the straight lines as shown in Fig.5. On these lines we plot three points for each object, indicating their U and Vs when adopting radial velocity 0 and ± 30 km/s. Since all space velocities are located within the 2σ circle, it is likely that these three L dwarfs are disk objects.

To further quantify the possibility of the three L dwarfs without measured radial velocity being halo component, we calculate two "critical" radial velocities (expressed as V_{rad1} and V_{rad2}) which locate the U and V velocities on the 2σ circle. Considering their radial velocity distribution, integrate the Gaussian profile of the radial velocity outside the two points V_{rad1} and V_{rad2}, we then obtained probabilities for the three objects being halo

component, which are listed in Table 7. These three objects have small probabilities of being halo component. So we conclude that our five L dwarfs are likely disk objects.

We use the test from Section 5 of Marocco et al. (2010) to see if these objects are very young. Younger stars have a small space velocity dispersion and hence small space velocities. Objects with U between -20 and 50 km/s, V between -30 and 0 km/s , W between -25 and 10 km/s will be younger than 0.5 Gyr. With the U,V and W ranges presented in Table 6 it is unlikely that these objects are younger than 0.5 Gyr.

4.3.   Comparison with model predictions

In Fig. 6 we plot our objects on color versus absolute magnitude diagrams. Model tracks from Burrows, Sudarsky & Hubeny 2006 (hereafter BSH06) and Allard et al. 2009 (http://phoenix.ens-lyon.fr/Grids/BT-Dusty/, hereafter BT-Dusty) are overplotted for comparison. The BSH06 model grids cover log(g) of 4.5, 5.0, and 5.5 (gravities in cgs) and effective temperatures from 700 K to 2200 K, with metallicity of [Fe/H] = -0.5, 0, +0.5. The BT-Dusty model grids cover log(g) of 4.5, 5.0, 5.5 and effective temperatures from 1500 to 3500 K, with metallicities of [Fe/H] = -0.5, 0.0, +0.5. The synthetic colors and absolute magnitudes are derived convolving the model spectra with the 2MASS filter profiles (see Marocco et al. 2010). The BSH06 model grids supply the flux at the surface of the object and at 10 pc. The latter calculation assumes the radius-log(g)-T_{eff} relation from Burrows et al. (1997). The BT-Dusty model grids only provide the flux at the surface of the object, so, to calculate the absolute magnitudes, we calculate the radius associated with each model spectrum by interpolating the BT-Dusty isochrones.

From Fig. 6 we can see the BSH06 and BT-Dusty can fit the colors of these L dwarfs. In principle, we could determine metallicity or gravity information from them. But because

of the known degeneracy between gravity and metallicity, our objects can be described by different combinations of the two parameters. This prevents assignment of a single gravity or metallicity based only on this diagram. Nonetheless, our targets can be fitted by solar or higher metallicity with log(g) between 5.0 and 5.5. This is consistent with the thin disk membership found in Section 4.2. We note that SD1717+6526 seems located outside the BT-Dusty model tracks. SD1717+6526 is an L4, so we tentatively conclude that BSH06 and BT-Dusty are more consistent at high temperatures ($\sim$2100 K) than at lower temperatures ($\sim$ 1700 K). We will investigate this further in the Section 5.3.

5. Temperatures and Luminosities

In this section we derive effective temperature, bolometric luminosity, radius, gravity and mass using the Chabrier et al. (2000, hereafter CBA00) dusty evolutionary model. Then we combine observational spectra with synthetic spectra from two brown dwarf models(BSH06 or BT-Dusty respectively) and the Stefan-Boltzmann law to estimate temperatures and luminosities.

5.1. Physical parameters from an evolutionary model

We directly found the effective temperature and other parameters for all our targets using the CBA00 dusty evolutional models and our derived parallax. The gravity of our targets are between log(g)=5.0 and 5.5 (see Section 4.3). Given that these objects have higher gravity than young field dwarfs (e.g. Cruz, Kirkpatrick & Burgasser 2009), and following our findings in Section 4.2, we assume our targets to be between 0.5 and 10 Gyr old. For this age range the dusty evolutionary model CBA00 provides relations between M_K and effective temperature, radius, bolometric luminosity, gravity and mass (Fig. 7).

Combining our parallax with 2MASS magnitudes we obtain M_K and using CBA00 we find the parameters listed in Table 8.

5.2. Temperatures and Luminosities from the Stefan-Boltzmann law

We have obtained both optical (from Cruz et al. 2007) and infrared (from Cruz et al. 2013; Burgasser et al. 2008b, 2010) spectra for three of our targets: 2M0141+1804, 2M1807+5015 and 2M2242+2542. To calibrate the spectra in flux, we used the z band magnitude (for 2M1807+5015 we use $z_{\rm est}$ in Table 1) in the optical, and 2MASS J band photometry in the near-infrared. To calculate the bolometric flux, we combined the observational spectra with the BSH06 and the BT-Dusty models. We calibrated the flux level of the model spectra using WISE W1 magnitudes, since these are well calibrated long wavelength measurements and allow the spectra to join reasonably with the observed K band. To calculate an effective temperature range, following a similar method to Marocco et al. (2010), we use the classical Stefan-Boltzmann law and the relationship between $F_{\rm bol}$, $L_{\rm bol}$ and $T_{\rm eff}$

$$F_{\rm bol} = L_{\rm bol}/4\pi D^2, \quad L_{\rm bol} = 4\pi\sigma R^2 T_{\rm eff}^4 \tag{2}$$

Integrating the observed optical and near-infrared spectra we obtained a preliminary flux, which combined with our parallax yields a luminosity. Interpolating the CBA00 luminosity-radius relationship (see Fig. 7), we derived the model predicted radius for our targets. Having the radius and preliminary flux, we then obtained a preliminary effective temperature. For the moment we do not consider metallicity and gravity, this is discussed below. Using this temperature, we can choose the appropriate model spectra. We then integrated the spectral energy distribution (formed by optical, near-infrared and model

spectra) to recalculate the bolometric flux, and therefore a more precise temperature. Iterating the above procedure twice, we obtain the bolometric flux, luminosity and effective temperature listed in Table 9.

When we choose the model spectra for an object, for either BSH06 or BT-Dusty model spectra, we assume the targets have solar metallicity, and test two values of gravity: log(g)=5.5 and log(g)=5.0. Usually there are four models available, taking 2M1807+5015 for example, the preliminary temperature is between 1875 and 1985 K (see Table 9), and we choose the four synthetic spectra with closest model parameters amongst the grids available: in this case 1900K, log(g)=5.5; 1900K, log(g)=5.0; 2000K, log(g)=5.5; 2000K, log(g)=5.0. For each of the chosen model spectra we then overlap with our observational spectra in order to create a full energy distribution. We then output $F_{\rm bol}$, $L_{\rm bol}$, $T_{\rm eff}$ values. The smallest and largest values generated by this process enable us to find the range for each parameter given in columns 5-10 of Table 9. We note that the model grids available offer one or two synthetic spectra for each temperature which correspond to different values of log(g). Thus we are not in a position to estimate reliable gravities for our targets.

The uncertainty on temperature is calculated via standard propagation of the errors on flux, distance and radius. For 2M2242+2542, the flux errors in the optical and near-infrared bands were derived using the average flux errors of 2M0141+1804 and 2M1807+5015 since they are not available in the spectral file. The model spectra files do not provide the errors on flux. However, when calculating the effective temperature, we used BSH06 and BT-Dusty model grids to locate the appropriate synthetic spectra for each object and so find the uncertainty on the synthetic spectra flux. So that we can calculate the uncertainty on bolometric flux. To determine the error on radius we use the spread between the two values derived from the CBA00 evolutionary model (see Table 9). The final temperature errors obtained are listed in columns 7 and 10 of Table 9. We note that the uncertainties on

temperatures reflected the ranges of the temperatures, which are dominated by the radius errors, Burgasser et al. (2008a) find the same conclusion with a similar approach although they did a piecewise scaling of the model spectra using multi-band photometry.

5.3. Comparison

A comparison of the temperatures in Tables 8 and 9 indicates that they are consistent for each individual object. Effective temperatures using the BSH06 and BT-Dusty models are very close for 2M0141+1804 and 2M1807+5015 with differences of ∼20 K. The three temperatures for 2M2242+2542 are consistent, but the differences between them are larger, which is also reflected by the large errors on temperature (see Table 9). The temperature from the BT-Dusty model is slightly higher than that from BSH06, which is close to the CBA00 one.

We should note that 2M2242+2542 is of spectral type L3, and is therefore clearly cooler and with different features from the other L1 targets. The flux of the BT-Dusty models does not join well with the observed spectrum, over-predicting the flux level at K band. We therefore expect the model flux to be higher than the object one in the mid-infrared as well, leading to an over-estimation of its $T_{\rm eff}$. We would conclude that for this object the fit given by the BT-Dusty models is not as accurate as the BSH06 one.

6. Comments on individual targets

2M0141+1804: Our results on temperature are consistent with Sengupta & Marley (2010) who estimate a temperature of 1850 ± 250 K using equations 3 and 4 of Stephens et al. (2009). The large error of 250 K is due to the difference in optical and IR spectral types and the authors used both values when calculating the temperature. Our

results have a smaller range in temperature, because we have the optical and near-infrared spectra, which allow us to get a relatively precise luminosity hence effective temperature. The radial velocity is 24.7 km/s reported by Blake, Charbonneau & White (2010). Our proper motions are within one sigma of those in Casewell et al. (2008) though ours are significantly more precise.

SD1717+6526: The proper motions are consistent with those of Faherty et al. (2009) and the photometric distance we calculated based on Dupuy & Liu (2012) is within one standard deviation of the trigonometric distance.

2M1807+5015: This object is the brightest of our five targets. Sengupta & Marley (2010) reported a T_{eff}=2100±100 K and Witte et al. (2011) derived T_{eff}=1900 K, $\log g$=5.5, [Fe/H]=0.0 through drift-phoenix model fitting. Our results are more consistent with the lower value. Seifahrt et al . (2010) reported a radial velocity of -0.4 km/s and very low values for the U,V,W velocity components, which is consistent with our results.

2M2238+4353: Bernat et al. (2010) reported it is a binary candidate with a mass ratio of 0.57-0.84 assuming an age between 1 and 5 Gyr. However we do not see any binary signature in our parallax determination residuals. Also, the position in Fig. 4 does not indicate binarity, though, unless the mass ratio is larger than about 0.6, we would not expect to see any significant brightening.

2M2242+2542: Bouy et al. (2003) observed this object using Hubble Space Telescope in a search for binaries and concluded it was a single object, which is consistent with our conclusions. Gizis et al. (2003) and Cruz et al. (2007) derived photometric distances of ~ 30 and ~ 27 pc respectively. We find a trigonometric distance of $\sim$21 pc which is consistent with the photometric distance from Table 3.

7. Summary and future work

We report the parallaxes and proper motions of five L dwarfs using a robotic telescope. Our trigonometric distances are very close to the photometric ones. Our proper motions are consistent with the literature but have smaller errors. Examinations of the objects' spectral type versus absolute magnitude, U versus V velocity and color versus absolute magnitude over-plotted with model tracks diagrams indicate that the five L dwarfs are single thin disk objects with solar metallicity. For all five objects, effective temperature, luminosity and bolometric flux, radius, gravity, and mass are derived from the CBA00 model. For three of our targets we derived the effective temperature combining their measured spectra with atmospheric models (BSH06 and BT-Dusty) to determine the bolometric flux. We found current low mass models do not work well at lower temperatures compared to higher temperatures. We find that BSH06 and CBA00 predict more consistent temperatures for the lower temperature objects than the BT-Dusty model but we also note our sample size is small and the error on T_{eff} is large when using BSH06. Further model testing with a bigger sample is needed to see if these effects are real.

This work is the first parallax determination using a ground-based robotic telescope. Parallax determinations have stringent observational requirements which are efficiently satisfied by robotic scheduling. The requirement for long term stability and repeatability is also well met by robotic procedures. The RATCam camera is scheduled to be completely decommissioned in 2013 and be replaced by the Infrared-Optical (IO) camera though RATCam and IO (with only a z-band filter) are both working currently. Once IO is fully commissioned, and, with the lessons learnt from this programme, we plan to launch a more ambitious programme to observe the nearby and rapidly expanding sample of interesting L and T dwarfs which are available for the Liverpool Telescope.

Acknowledgments

REFERENCES

Albert, L., Artigau E., Delorme P., et al., 2011, AJ, 141, 203

Allard, F., Hauschildt, P. H., Alexander, D. R., et al., 2001, ApJ, 556, 357

Andrei, A. H., Smart, R. L., Penna J. L. et al., 2011, AJ,141,54

Bensby, T., Feltzing, S. & Lundstrom, I., 2003, A&A, 410, 527

Berta, S., Rubele, S., Franceschini, A. et al., 2008, A&A, 488, 533

Bernat, D., Bouchez, A. H., Ireland, M. et al., 2010, ApJ, 715, 724

Blake, C. H., Charbonneau, D., White, R. J., 2010, ApJ, 723, 684

Bouy, H., Brandner, W., Martin, E.L. et al., 2003, AJ, 126, 1526

Burgasser, A. J., Vrba, F. J., Lepine, S., et al., 2008a, ApJ, 672, 1159

Burgasser, A. J., Liu, M. C., Ireland, M., J. et al., 2008b, ApJ, 681, 579

Burgasser, A. J., Cruz, K. L., Cushing, M., et al., 2010, ApJ, 710, 1142

Burgasser, A.J., 2011, ASPC, 450, 113B

Burrows, A., Marley, M., Hubbard, W. B. et al., 1997, ApJ, 491, 856

Burrows, A., Sudarsky, D., & Hubeny, I., 2006, ApJ, 640, 1063

Casewell, S. L., Jameson, R. F.& Burleigh, M.R., 2008, MNRAS, 390, 1517

Chabrier G., Baraffe I., Allard F. & Hauschildt P., 2000, ApJ, 542, 464

Cruz, K. L., Reid, I. N., Liebert, J. et al., 2003, AJ, 126, 2421

Cruz, K. L., Reid, I. N., Kirkpatrick, J.D. et al., 2007, AJ, 133, 439

Cruz, K. L., et al., 2013, in preparation

Cruz, K. L., Kirkpatrick, J. D. & Burgasser, A. J., 2009, AJ, 137, 3345

Dahn, C. C., Harris, H. C., Vrba, F. J., et al., 2002, AJ, 124, 1170

Delfosse, X., Tinney, C. G., Forveille, T. et al., 1997, A&A, L25, L28

Dupuy, T. J. & Liu, M. C., 2012, ApJS, 201, 19

Emerson, J. P., 2011, ASPC, 232, 339

Faherty, J. K., Burgasser, A. J., Cruz, K. L. et al., 2009, AJ, 137, 1

Faherty, J. K., Burgasser, A. J., Walter, F.M. et al., 2012, ApJ, 752, 56

Gizis, J. E., Reid, I. N., Knapp, G. R. et al., 2003, AJ, 125, 3302

Hawley, S. L., Covey, K. R., Knapp, G. R. et al., 2002, AJ, 123, 3409

Jameson, R. F., Casewell, S. L., Burleigh, M. R. et al., 2008, MNRAS, 384, 1399

Jao, W., Henry, T. J., Beaulieu, T. D. et al., 2008, AJ, 136, 840

Jones, H. R. A., Steele, I. A., 2001, udns.conf, J:Ultracool Dwarfs: New Spectral Types L and T

Kirkpatrick, J. D., Reid, I. E., Liebert J. et al. 1999, ApJ, 519, 802

Kirkpatrick, J. D., 2005, ARA&A, 43,195

Lawrence, A., Warren, S .J., Almaini, O. et al., 2007, MNRAS, 379, 1599

Leggett, S. K., Allard, F, Geballe, T. R. et al., 2001, ApJ, 548, 908

Leggett, S. K., Golimowski, D. A., Fan, X. et al., 2002, ApJ, 564, 452

Liu, M. C., Leggett, S. K., Golimowski, D. A. et al., 2006, ApJ, 647, 1393

Marocco, F., Smart, R. L., Jones, H. R. A. et al., 2010, A&A, 524, 38

Mendez, R. A. & van Altena, W. F., 1996, AJ, 112, 655

Monet, D. G., Dahn, C. C., Vrba, F. G. et al., 1992, AJ, 103, 638

Monin, J. L., Guieu, S., Dougados, C. et al., 2007, A&A, 211, 1222

Murray, D. N., Burningham B., Jones, H. R. A. et al., 2011, MNRAS, 414, 575

Oppenheimer, B. R., Hambly, N. C., Digby, A. P. et al., 2001, Science, 292, 698

Reid, I. N., Sahu, K. C., & Hawley, S. L., 2001, ApJ, 559, 942

Schmidt, S. J., Cruz, K. L., Bongiorno, B. J. et al., 2007, AJ, 133, 2258

Schonrich, R., Binney, J. & Dehnen, W., 2010, MNRAS,403, 1829

Sengupta, S. & Kwok, S., 2005, ApJ, 625, 996

Sengupta, S. & Marley, M. S., 2010, ApJ, 722, 142

Seifahrt, A., Reiners, A., Almaghrbi, K. A. M. et al., 2010, A&A, 512, 37

Skrutskie, M. F., Cutri R. M., Stiening R. et al. 2006, AJ, 131, 1163

Smart, R. L., Lattanzi, M. G. & Drimmel, R., 1999, Astrophysics and Space Science Library, 212, 195

Smart, R. L., Bucciarelli, B., Lattanzi, M. G. et al., 1999, A&A, 348, 563

Smart, R. L., Lattanzi, M. G., Bucciarelli, B. et al., 2003, A&A, 404, 317

Smart, R. L., Lattanzi, M. G., Jahreiβ, H. et al., 2007, A&A, 464, 787

Soubiran, C., Bienayme, O. & Siebert, A., 2003, A&A, 398, 141

Steele, I., Smith, R. J., Rees, P. C. et al., 2004, Proc. SPIE, 5489, 679

Stephens, D. C., & Leggett, S. K., 2004, PASP, 116, 9

Stephens, D. C., Leggett, S. K., Cushing, M. C. et al., 2009, ApJ, 702, 154

Stone, R. C., 2002, PASP, 114, 1070

Tata, R., Martin, E. L., Sengupta, S. et al., 2009, A&A, 508, 1423

West, A. A., Morgan, D. P., Bochanski, J. J. et al., 2011, AJ, 141, 97

Wilson, J. C., Miller, N. A., Gizis, J.E. et al., 2003, IAUS, 211, 197

Witte, S., Helling, C., Barman, T.et al., 2011, A&A, 529, 44

Wright, E., Eisenhardt, P. R. M., Mainzer, A. K. et al., 2010, AJ, 140, 1868

York, D. G., Adelman, J., Anderson, JrJ. E., et al., 2000, AJ, 120, 1579

Zapatero Osorio, M. R., Caballero, J. A. & Bejar, V. J. S., 2005, ApJ, 621, 445

Zhang, Z. H., Pokorny, R. S., Jones, H. R. A. et al., 2009, A&A, 497, 619

Zhang, Z. H., Pinfield, D. J., Day-Jones, A. C. et al., 2010, MNRAS, 404, 1817

Table 1.   Magnitudes and spectral types of the targets.

Short Name	Discovery Name	z_{SDSS}	z_{est}	J_{2MASS}	H_{2MASS}	K_{2MASS}	W1	SpT_{opt}	SpT_{NIR}
2M0141+1804	2MASS J0141032+180450	16.34	*16.34*	13.88	13.03	12.49	12.16	L1[1]	L4.5[3]
SD1717+6526	SDSS J171714.10+652622.2	17.79	*17.67*	14.95	13.84	13.18	12.53	L4[2]	-
2M1807+5015	2MASSI J1807159+501531	-	*15.43*	12.93	12.13	11.60	11.25	L1.5[4]	L1[3]
2M2238+4353	2MASSI J2238074+435317	-	*16.42*	13.84	13.05	12.52	12.20	L1.5[4]	-
2M2242+2542	2MASS J22425317+2542573	17.49	*17.42*	14.81	13.74	13.05	12.51	L3[1]	L[1]

[a]z_{est} is an z-band magnitude estimated from the z-J color - optical spectral type relation from Zhang et al. (2009). SpT_{opt} is the spectral type obtained from optical spectra and SpT_{NIR} from the near infrared spectra.

References. [1]Cruz et al. (2007); [2]Hawley et al. (2002); [3] Wilson et al. (2003); [4]Cruz et al. (2003); [5]Zhang et al. (2010).

Table 2.   Parallaxes and proper motions derived for our targets.

| Short Name | RA,Dec | Epoch | N_o, N_r | Δt | π | COR | $\mu_\alpha cos\delta$ | μ_δ | V_{tan} |
	(hh mm ss),(dd mm ss)			(yrs)	(mas)	(mas)	(mas/yr)	(mas/yr)	(km/s)
2M0141+1804	01:41:03.5,+18:04:49.5	2008.66	40,9	4.35	44.06±2.05	1.77	405.2±1.1	-48.7±0.9	43.9±2.0
2M1717+6526	17:17:14.2,+65:26:21.2	2008.60	65,5	7.62	57.05±3.51	1.46	150.2±1.0	-109.3±0.6	15.4±1.0
2M1807+5015	18:07:15.9,+50:15:30.2	2009.27	57,18	7.04	77.25±1.48	1.68	27.2±1.0	-130.2±1.5	8.1±0.2
2M2238+4353	22:38:07.7,+43:53:16.6	2009.49	52,37	7.71	54.11±1.55	1.24	324.3±0.5	-121.0±0.4	30.3±0.9
2M2242+2542	22:42:53.4,+25:42:56.6	2009.53	53,11	7.83	47.95±2.74	1.71	382.0±0.9	-64.6±0.7	38.3±2.2

[a]The columns denote object name, right ascension (RA) and declination (Dec) of the base frame, epoch of the base frame, number of frames and number of reference objects(N_o, N_r), total time span for observations (Δt), absolute parallax (π), correction from relative to absolute parallax (COR), proper motions in RA($\mu_\alpha cos\delta$), proper motion in Dec(μ_δ) and tangential velocity(V_{tan}).

Table 3.   Photometric and trigonometric distances of the five L dwarfs.

Short Name	D_J	D_H	D_K	$< D_P >$	D_π
	(pc)	(pc)	(pc)	(pc)	(pc)
2M0141+1804	24.2±4.2	24.2±4.2	22.6±3.9	23.7±4.1	22.7±1.1
SD1717+6526	22.9±3.4	22.0±3.3	20.3±3.2	21.7±3.3	17.5±1.7
2M1807+5015	14.4±2.5	14.9±2.6	14.0±2.4	14.4±2.5	12.9±0.3
2M2238+4353	21.9±3.8	22.7±4.0	21.3±3.6	22.0±3.8	18.5±0.6
2M2242+2542	26.1±3.9	24.8±3.7	21.9±3.4	24.2±3.7	20.9±1.2

[a]We calculated the spectrophotometric distances according to the J,H and K band SpT - absolute magnitude relationship of Dupuy & Liu (2012). $< D_P >$ is the weighted mean spectrophotometric distance and D_π is the distances derived from our trigonometric parallax.

Table 4.   Comparison of our proper motions with literature values.

Short Name	Table 2 $\mu_\alpha cos\delta, \mu_\delta$	Literature $\mu_\alpha cos\delta, \mu_\delta$
	(mas/yr)	(mas/yr)
2M0141+1804	405.2±1.1, -48.7±0.9	425.1±17.6,-32.2±16.5[1]
SD1717+6526	150.2±1.0, -109.3±0.6	159.0±7.0, -92.0±16.0[3]
2M1807+5015	27.2±1.0, -130.2±1.5	34.6±18.5,-125.7±14.3[2]
2M2238+4353	324.3±0.5, -121.0±0.4	324.0±12.0,132.0±16.0[3]
2M2242+2542	382.0±0.9, -64.6±0.7	408.8±15.5,-45.2±16.2[2]

[a]References.   [1]Casewell, Jameson & Burleigh   (2008), [2]Jameson et al.   (2008),[3]Faherty et al.   (2009)

Table 5.   Coefficients of equation 1 fitting objects in figure 4 excluding known and possible
binaries.

Mag.	a_0	a_1	a_2	a_3	a_4	a_5	a_6	σ
M_J	-1.33315e2	5.33338e1	-7.99504	6.21422e-1	-2.6167e-2	5.64852e-4	-4.88497e-6	0.456012
M_H	-8.62209e1	3.48403e1	-5.12332	3.93049e-1	-1.64117e-2	3.53139e-4	-3.06005e-6	0.400478
M_K	-1.24473e2	4.98554e1	-7.50172	5.85077e-1	-2.47521e-2	5.37504e-4	-4.67296e-6	0.403721

Table 6.   Calculated U, V and W for our five targets.

Short Name	V_{rad} km/s	U km/s	V km/s	W km/s
2M0141+1804	24.7	-56.6	-6.2	-5.0
	30	-3.1	44.0	15.2
SD1717+6526	-30.0	1.6	-5.3	-18.6
	0.0	-0.8	19.4	-1.7
2M1807+5015	-0.4	-3.5	11.7	4.4
	30.0	-33.9	33.0	-22.3
2M2238+4353	-30.0	-24.8	-24.8	-8.9
	0.0	-29.3	4.1	-15.6
	30.0	-39.4	26.2	-29.8
2M2242+2542	-30.0	-39.6	-26.4	-1.0
	0.0	-39.5	-0.1	-15.4

[a]Note. We assume the three L dwarfs without mea-
sured radial velocities to be 0 and $\pm$ 30 km/s as radial
velocities following the SDSS M dwarfs' distribution.

Table 7. "Critical" radial velocities and halo probabilities.

Short Name	V_{rad1}	V_{rad2}	P
	km/s	km/s	%
SD1717+6526	-179.1	48.0	5.5
2M2238+4353	-137.8	49.2	5.1
2M2242+2542	-136.9	57.6	2.8

[a]Note. These radial velocities for the three targets locate them on the 2 σ ellipsoid in Fig. 5. Integrating the Gaussian profile of the radial velocity outside the 2σ velocities for each target we get the probability(P) that the targets are halo objects.

Table 8. Temperature, luminosity, radius, gravity and mass derived from CBA00 model.

Short Name	M_k	T_{eff}	Luminosity	Radius	Gravity	Mass
		(K)	$log_{10}(L/L_\odot)$	$R/R_\odot$	$log_{10}(g)$	$M/M_\odot$
2M0141+1804	10.71	2225-2305	-3.63-(-3.60)	0.1000-0.1055	5.21-5.34	0.067-0.080
SD1717+6526	11.96	1450-1563	-4.41-(-4.36)	0.0860-0.1040	5.00-5.41	0.040-0.070
2M1807+5015	11.04	2000-2138	-3.82-(-3.78)	0.0958-0.1036	5.18-5.36	0.058-0.077
2M2238+4353	11.19	1828-2038	-3.95-(-3.85)	0.0930-0.1030	5.15-5.37	0.053-0.075
2M2242+2542	11.45	1688-1850	-4.14-(-4.08)	0.0905-0.1032	5.08-5.39	0.048-0.073

[a]The range of values shown are found based on assuming age range between of 0.5 and 10 Gyr.
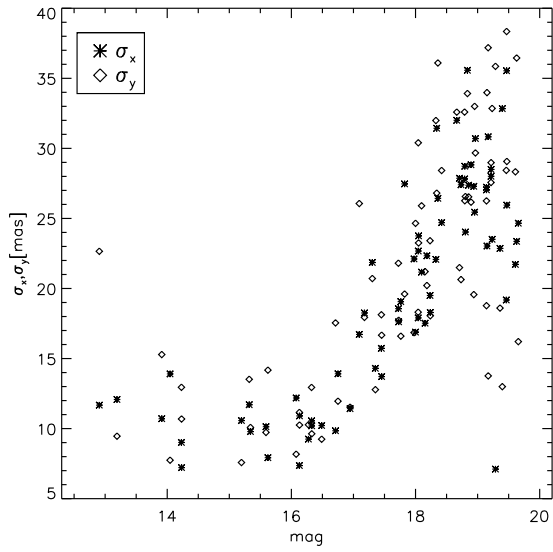
Fig. 1.— σ_x,σ_y of the x,y coordinates for common objects in 57 frames of the 2M1807+5015 field. The frames were made over 19 nights spanning $\sim$7.04 years. On the x axis we plot apparent magnitude in the z band and on the y axis we plot the σ_x,σ_y in mas. The median σ_x,σ_y are 21,21 mas for all objects and 11,11 mas for objects with z band magnitude brighter than 17.

Table 9.   Bolometric flux, luminosity, effective temperature from combination of observational and model spectra.

	Preliminary Parameters			Combining BSH06			Combining BT-Dusty		
Short Name	L	$R/R_\odot$	$T_{\rm eff}$	$F_{\rm bol}$	$L_{\rm bol}$	$T_{\rm eff}(\sigma)$	$F_{\rm bol}$	$L_{\rm bol}$	$T_{\rm eff}(\sigma)$
2M0141+1804	-3.80	0.1038-0.0950	2015-2107	1.24-1.24	-3.69	2126-2206(101)	1.30-1.30	-3.68	2147-2216(105)
2M1807+5015	-3.93	0.1030-0.0919	1875-1985	2.83-2.84	-3.83	1982-2071(68)	2.97-2.98	-3.81	1999-2085(69)
2M2242+2542	-4.24	0.1035-0.0885	1560-1687	0.618-0.624	-4.11	1699-1823(225)	0.715-0.751	-4.03	1736-1844(133)

[a]Notes. Columns 2-4 are preliminary parameters: luminosity, radius in $R_\odot$, effective temperature ($T_{\rm eff}$). Columns 5-7 and Columns 8-10 are final parameters after two iterations combining BSH06 and BT-Dusty respectively: bolometric flux, luminosity and temperature. Luminosity is in units of $log_{10}(L/L_\odot)$, bolometric flux $F_{\rm bol}$ in units of $(x10^{-14}J/m^2)$ and temperature in units of K.
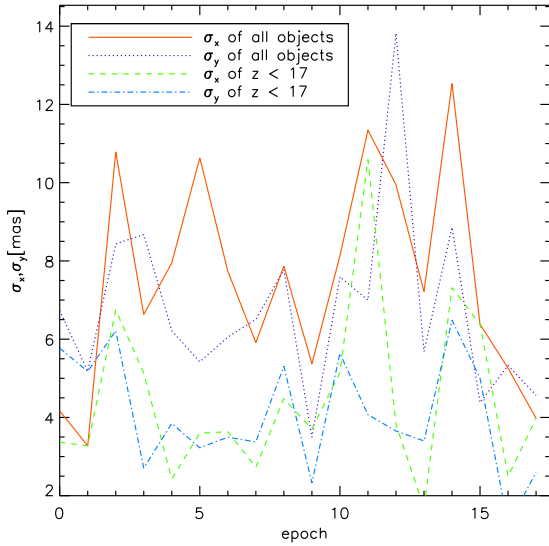

Fig. 2.— σ_x,σ_y of the x,y coordinates for objects in the 2M1807+5015 field as a function of epoch sapnning 7.04 years. The σ_x,σ_y are calculated using three sequential images from each of the 19 nights. The σ_x,σ_y along the y axis are median value of the corresponding epochs for two subsets: (1) all objects detected and (2) objects detected brighter than 17 in z magnitude. The median precisions among the 19 epochs for all objects are 7.7,6.5 mas and for the $z < 17$ subset are 3.8,3.7 mas in σ_x,σ_y respectively.
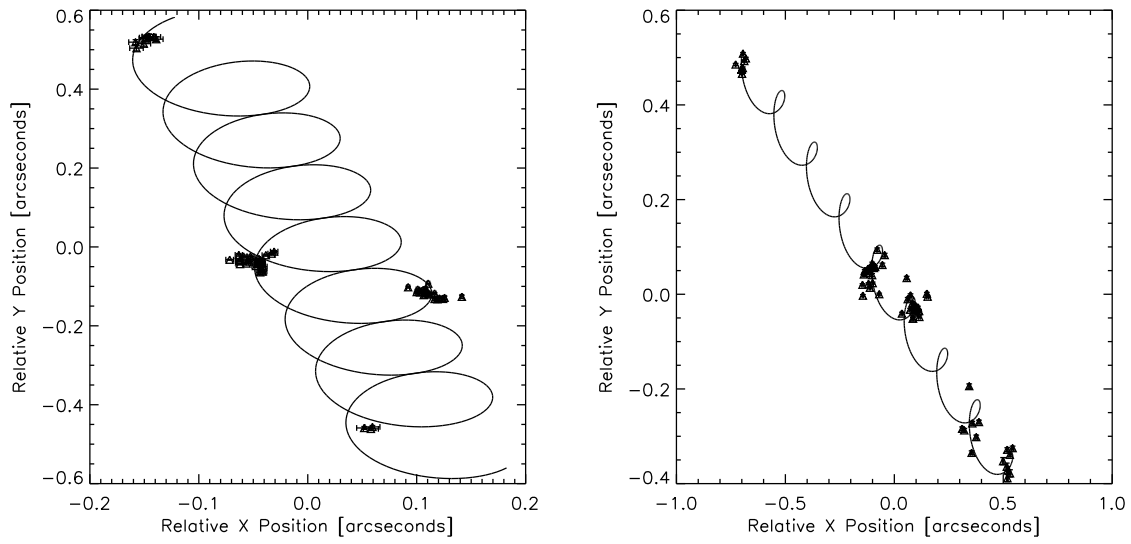
Fig. 3.— Observations of 2M1807+5015 (left) and 2M2238+4353 (right) using CASU centroids along with our solutions over plotted.
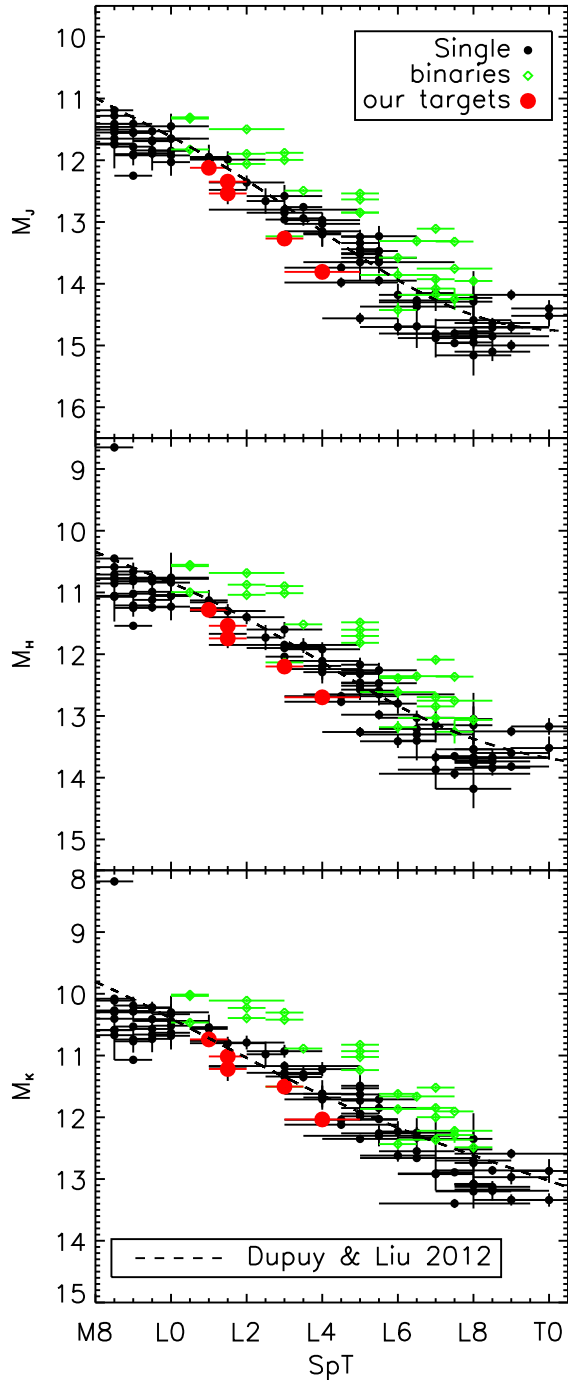
Fig. 4.— 2MASS JHK absolute magnitude as a function of optical spectral type. The black solid circles and the blue diamonds are objects from Dupuy & Liu (2012) with published parallaxes. Black solid circles are M8.5 to T0 dwarfs without indication of binarity, blue diamonds are unresolved binaries. The red triangls are our five targets. Including our five targets, in total 84 single objects are used when fitting the solid red polynomial curve. Dupuy & Liu (2012) relations are over-plotted as dashed lines.
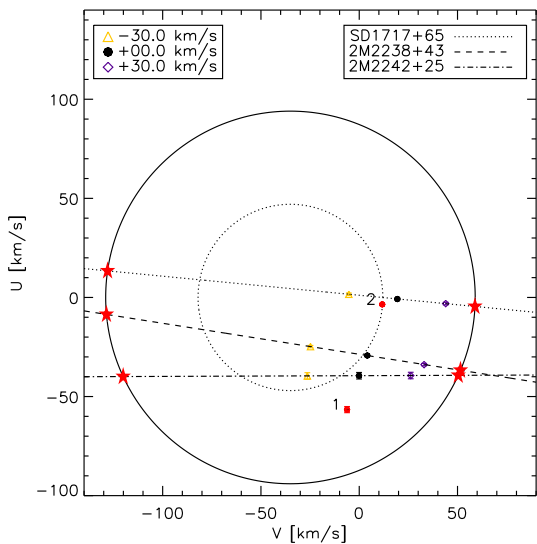
Fig. 5.— U versus V Galactic velocities. The dotted and solid ellipses are 1 and 2σ velocity ellipsoid for disk sars according to Reid, Sahu & Hawley (2001). The coordinates of the center are (-35,0) km/s (Oppenheimer et al. 2001); the radius is 47 km/s and 94 km/s. The red filled circles labeled 1 & 2 are 2M0141+1804 and 2M1807+5015 which have measured radial velocities. For the other objects the dotted, dashed dot and dashed lines describe the U and V velocities when adopting different radial velocities. Their U and V velocities when using 1σ and mean radial velocity 30, 0, -30 km/s are shown on each line. The asterisks located on the 2 sigma ellipse indicate U and V velocities from the "critical" radial velocities listed in Table 7.
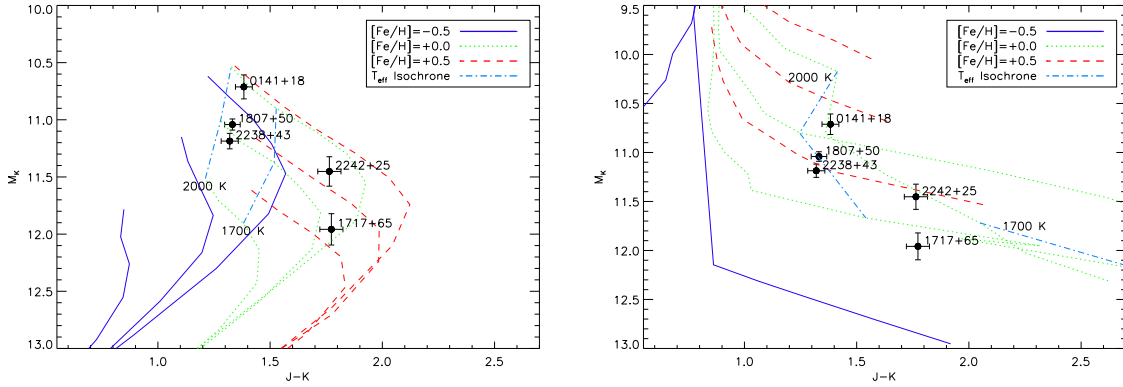
Fig. 6.— Color-M_K diagrams of our five L dwarfs with models. The model tracks are the BSH06(left) and BT-Dusty(right) models. Different line-styles indicate different metallicities. For each metallicity, the 3 curves indicate different gravity. The gravity increases from bottom-left to top-right with values of log(g)=4.5, 5.0, 5.5. Thus, for a given mass evolutionary track, higher gravity models have fainter (larger) values of M_K and redder (larger) values of color. All magnitude are in 2MASS system.
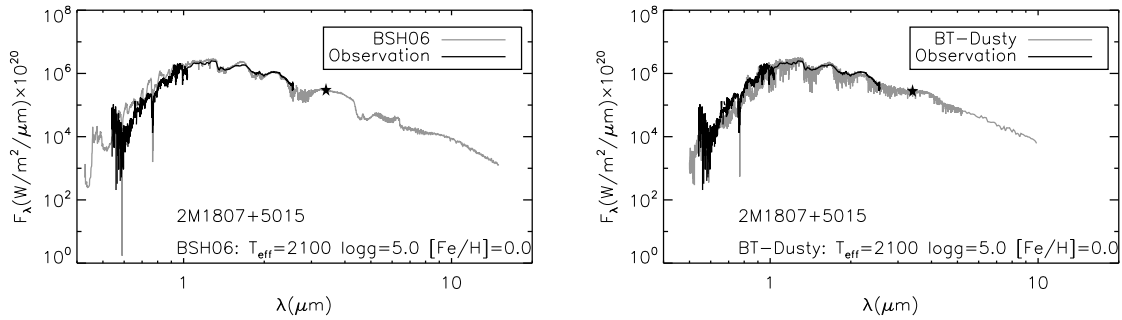

Fig. 7.— Left: absolute magnitude-effective temperature diagram. Right: luminosity-radius diagram. The two diagrams are plotted according to the CBA00 dusty evolutionary model assuming ages of our targets between 0.5 and 10 Gyr. For this age range, the targets' radius change only $\sim 5\%$. Interpolating the derived M_K or luminosity we can find the effective temperature or radius.